RESEARCH

Analyses of the brown stain on the Parthenon Centaur head in Denmark

Kaare Lund Rasmussen[1*], Bodil Bundgaard Rasmussen[2], Thomas Delbey[3], Ilaria Bonaduce[4], Frank Kjeldsen[5] and Vladimir Gorshkov[5]

Abstract

In 1688 two sculptural fragments, a head of bearded man and a head of an unbearded youth, arrived in Copenhagen, sent from Athens as a gift to King Christian 5. They were placed in the Royal Kunstkammer, their provenance given as the Temple of Artemis in Ephesos, one of the Seven Wonders of the World. Almost a hundred and fifty years later, in the early 1820's they were noticed and studied by two scholars independently visiting the Kunstkammer. However, both concluded that the two heads belonged to one of the metopes decorating the south side of the Parthenon temple on the Acropolis in Athens, showing fighting between Greeks and the mythical Centaurs, part man and part horse. In the 1830's another sculptural fragment, a horse's hoof, obtained through the German archaeologist and state antiquary of Greece, Ludwig Ross, reached Copenhagen. It was forwarded by the Danish consul to Athens, C.T. Falbe, as a gift to King Christian 8. The inventory reads: '… was found on the Acropolis near the Parthenon temple and is supposed to belong to one the Centaurs on the metopes.' The present paper focuses solely on the head of the Centaur.

A brown stain was noticed on the Parthenon marbles as early as 1830 by the British Museum and has ever since eluded a deeper understanding of its genesis despite many investigations and attempts of analyses. A quite similar brown stain can be observed on the Centaur's head in Copenhagen as well.

The present study reports analyses by LA-ICP-MS, SEM–EDX, μXRD, GC–MS, and LC–MS-MS, as well as optical microscopy of five small samples sequestered in 1999 from the Centaur head curated by the National Museum of Denmark. Our analyses show that the brown stain consists of two consecutively added surficial layers of the calcium oxalate minerals whewellite and weddellite. Despite a thorough search using proteomics, we have found no viable organic precursor material for the oxalates. Our results do not solve the mystery of the formation of the brown stain, but they do further qualify the structure and characterization of the brown stain.

Keywords Parthenon temple, Athens, Brown stain, Centaur head

*Correspondence:
Kaare Lund Rasmussen
klr@sdu.dk
Full list of author information is available at the end of the article

Rasmussen *et al. Heritage Science*   (2024) 12:18

Page 2 of 17

Introduction

The two marble heads in the Royal Kunstkammer in Copenhagen were mentioned in its earliest extant inventory initiated by order of King Christian 5 in 1687. Holger Jacobaeus, professor of anatomy at the University of Copenhagen was entrusted with the task. Jacobaeus completed his inventory in Danish in 1689 [1]. The entry of interest here reads as follows: 'Toe Hofveder af Marmor som hafver staaet i Dianae Tempell till Epheso, fremskichet af Capitain Hartmand fra Athenen Anno 1688'. (In English: 'Two heads of marble that have stood in the Temple of Diana in Ephesos, sent by Captain Hartmand from Athens in the year 1688'.).

The handwritten manuscript was translated into Latin and printed with amendments, additions, and engravings in Copenhagen in 1696 under the title *Museum Regium*. In this edition the entry on the two heads differs significantly from the first one given: 'Capita duo MARMOREA, qvae in templo qvodam reperta. Athenis anno 1688 huc translatae sunt'. (In English: 'Two heads, that were found in some temple. Sent from Athens in the year 1688') [1].

Holger Jacobaeus had now changed the entry as he had probably realized that the heads could not possibly be from the Artemis/Diana temple in Ephesos, which was set aflame by an arsonist in the fourth century BC and then fell into oblivion. By the seventeenth century the temple was only known from ancient literary sources and phantasy paintings. Jacobaeus also left out the name of the sender 'Capitain Hartmand', probably due to lack of information about him. When eventually, the heads were identified as belonging to the Parthenon, in 1825 by the German art historian, Karl F. von Rumohr, and in 1827 by the Danish archaeologist P.O. Brøndsted, neither managed to identify 'Capitain Hartmand'.

Karl F. von Rumohr visited the Kunstkammer in Copenhagen in the autumn of 1825, and published a short report on his visit in 'Kunstblatt', a German weekly magazine on art, where he was brief but to the point. He states his observation, as follows (our translation from German): 'Among the not numerous ancient objects (in Copenhagen) are however, some fragments from Athens – the upper part of a Centaur from the metopes of the Parthenon and a head, which, judging from the grove around his head must once have had a metal headband'. [2].

In 1827 the Danish archaeologist P.O. Brøndsted, who in the 1820's stayed mainly in Rome, Paris, and London, had a short sojourn in Copenhagen. During this he paid a visit to the Kunstkammer, where he realised that the two heads of marble in the collection had belonged to the Parthenon temple in Athens. In 1828 he brought casts of the heads to London and presented them to the British Museum. In the accompanying letter he wrote:

> *Having recognised last year when I was in Copenhagen, that two very fine heads of Pentelic marble, which were sent from Athens in the year 1688 by Captain Hartmand and presented to the King of Denmark's Museum, belonged to the exterior frieze on the southern side of the temple, I suppose it to be of some interest to those who study the Athenian marbles in the B.M. to compare the Copenhagen fragments with the remaining metope.*

Brøndsted failed in joining the heads to the correct metope, no. 4 counting from the southwest corner [3]. Neither did he make his discovery publicly known until 1830, the year the second volume of his renowned report on his travels and studies of monuments in Greece [4] was published in a French and a German edition. He dedicated the volume to a study of the Parthenon and its sculptures in the British Museum and published the heads in Copenhagen as part V, accompanied by a beautiful engraving [4, 5]:170–188.

The credit for having shed some light on the elusive 'Capitain Hartmand' goes to the Danish historian Louis Bobé (1857–1951), who identified him, researched, and published his biography. The title he gave it, 'Moritz Hartmann. Captain of the Danish and Venetian Navy—Awarded the Order of San Marco and Governor of Trankebar' covers his life's achievements very well [6]. Here it will suffice to take a brief look into his younger years.

Moritz Hartmann was born 1656 in the small town of Heiligenhafen in Schleswig–Holstein, at that time part of Denmark. As a young man he enjoyed an education at the Danish School of Navigation established in 1679 in Copenhagen. After serving some years in the Danish Navy and having risen to the rank of captain, Hartmann obtained permission from the King to 'travel for some time abroad in order to better himself in his service at home.'

Thus, the Danish captain signed up as a volunteer in the Venetian Navy in the summer of 1685, at a time when the Venetians had initiated their military campaigns against the Ottoman Empire. He served in both the navy and the infantry, his courage being exceptional on several occasions and especially so in the battle of Kalamata in 1685, after which he in 1686 was awarded the Order of San Marco. Instrumental in this was the recommendation of his commanding officer Colonel von Tuppau given after the battle.

> *I, Giovanni Bernardo Topao, Colonel of the Saxon*

Rasmussen *et al. Heritage Science* (2024) 12:18

Page 3 of 17

troops hereby certify, that as the entire army landed at Calamata and the Venetian troops attacked the Turkish army, Mr. Mauricio Artmant demonstrated great courage and ability, endangering his own life. I hereby bear witness that he excelled in an honourable way and earned general praise.

Signed: *The camp at Calamata 19 September 1685, Hans Bernhardt von Tuppau.* [6]:72.

After the victory at Kalamata Morosini continued his expedition and had his eyes set on Athens as a place for the troops to spend the winter. The Venetian fleet arrived at Porto Leone in Piraeus on September 21st, 1687. The army came over land from their camp at the Isthmus and made camp by the Kephissos river. The Greeks sent envoys to negotiate an occupation of Athens by the Venetians as support against the Turks. These, however, had retreated to the Acropolis, soldiers and civilians alike, so an attack on this, their stronghold, seemed inevitable. Adding to the future disaster was the fact, that the Turks used the western part of the Temple for storing ammunition.

In conclusion let us give the stage to an eyewitness of the catastrophic event, the Swedish lady Anna Aakerhjelm, who was part of the entourage of Field Marshall Count Otto Wilhelm Königsmarck, in charge of the Venetian army. But first a few words on Anna Aakerhjelm:

Anna Aakerhjelm was born in 1642 in Södermanland in Sweden, she and her several siblings were orphaned when still very young, but by supporting each other all managed to get an education, Anna's focusing on Latin and modern languages. This accomplished, Anna was employed as a lady companion to Countess Catherina Charlotta De la Gardie, who in 1682 married Count Otto Wilhelm Königsmarck. When Count Königsmarck joined the Venetians in their quest against the Ottoman Empire as Field Marshall to Francesco Morosini, he brought along his wife, so Anna followed suit. During the campaign of Morea culminating in the bombardment on Athens, Anna Aakerhjelm kept a diary and wrote several letters to her brother, Samuel Aakerhjelm of which, sadly, only few have survived [7].

The following letter (translated from Swedish) sent to her brother Samuel, although very brief, offers a glimpse of her feelings upon seeing the temple, Königsmarck's subtle aversion to carrying out the inevitable, and Anna's sadness and frustration after the deed was done [7]:183.

Athens 28 September 1687
Dear Honoured Brother
The castle is on a hill, and it is said to be most difficult to conquer as no mining could be made: how little his Excellency wanted to destroy the beautiful

temple which has stood for 3000 years and is called Temple of Minerva, but to no avail, the bombs did their work and the Temple can never in this world be resurrected.
After eight days resistance the Turks put out a white flag after the Seraskier did not come to help. And it was granted that every man could take as much as he could carry to the sea – and that is six miles. Many left their burden on the road. Very fine sown linen clothing such as they use. The town is also better than any of the others we have been to, very pretty houses – the Greeks' as well as the Turks'. The Greeks surrendered to the Republic [Venice] when the army reached the town, but they have buried all their belongings. I cannot possibly describe all the antiquities here.

The most detailed and valuable account of the attack on the Acropolis is given by the Saxon Major General H. Ph. Ohr in a lengthy letter written just six days after the disastrous event to Duke Ernst August of Hannover [6]:87–90. This lengthy letter holds, however, no information on Moritz Hartmann being in Athens in September 1687. As a Captain in the Venetian navy, he clearly was in Athens as many other young Germans and Scandinavians who had enlisted in the Venetian army or navy. Sadly, as he did not keep a diary, we are, regarding the acquisition of the two marble heads left with just the note stating that the two heads were shipped from Athens due to become part of King Christian 5's Kunstkammer in Copenhagen.

Det Kongelige Kunstkammer later turned into the National Museum of Denmark, where the marbles are curated and exhibited to this day. Both the two heads and the hoof have a brown staining, sometimes called *patina* or more recently a film, mostly prominent on the side facing the wall - just like many of the other Parthenon marbles [8].

The brown stain was noticed as early as 1830, when the British Museum tried to ascertain if the brown stain originated from an original paint layer [9]. The conclusion at the time was that the brown stain was due to natural processes of (unspecified) atmospheric reactions, or of the migration of iron compounds from the interior of the marble to its surface. Opposing this, Penrose [10] suggested in 1851 that the brown stain was due to a wash of ochre, intended to tone down the piercing glare of white marble and that the brown stain was not the result of the oxidization of iron contained within the marble. In 1853 Justus Von Liebig [11] made the first scientific investigation of the brown stain ascertaining that it contained oxalates, later to be shown to be the two calcium oxalate minerals whewellite and weddellite. Since then, many

Rasmussen *et al. Heritage Science*   (2024) 12:18

Page 4 of 17

studies have reported the presence of calcium oxalates in brown stain on marble surfaces [12–18].

In 1987 Monte et al. [19] suggested that the whewellite ($CaC_2O_4 \cdot H_2O$) and weddellite ($CaC_2O_4 \cdot 2H_2O$) originated from precipitation from lichen growing on the surfaces of the marbles in the past, at a time when the climate was supposedly better suited to support lichen growth than nowadays. This view is somewhat supported by the observation that the brown stain on the marbles still residing in situ at the Acropolis until in recent years moved to the Acropolis Museum diminished from the 19th Century to the present day. Nineteenth century paintings, watercolours and photographs of the Acropolis monuments testify to this development [8]. Formation by other biological organisms such as algae, fungi, bacteria, and other microorganisms has also been suggested [20–22].

The brown stains of the Parthenon and the Erechtheion were thoroughly investigated by Polikreti and Maniatis [23] and Maravelaki-Kalaitzaki [24], who found the presence of both oxalates and hydroxyapatite which they concluded to be associated with the decomposition products of organic matter from ancient treatments applied to protect or tone the marble surface. Some of the samples studied by Maravelaki-Kalaitzaki showed a structure resembling the accumulation of windblown dust as part of the patina. In recent years it has even been suggested to use oxalates as a modern protective agent against deterioration of the marble surface [25–28].

In 2019 Laura Rampazzi [29] made a comprehensive review of the calcium oxalate films on buildings and works of art on a global scale, reporting the various analytical methods that have been applied, and the interpretations that have been presented through time. This review, balancing more than 300 scientific papers on the subject, concluded that the genesis of the brown stain could not yet be ascertained. The possibilities remain for a biological origin, an application of a layer – substrate or paint—in connection with the production of the piece of art in antiquity, a deposit from air pollution, or later conservation attempts.

The present study characterizes the brown stain from the Centaur head in Danish custody with Scanning Electron Microscopy with energy dispersive X-ray detection (SEM–EDX), Laser Ablation Inductively Coupled Plasma Mass Spectrometry (LA-ICP-MS), and capillary micro-X-ray Diffraction (μXRD). Furthermore, we have attempted to search for a biological progenitor for the oxalates by Gas Chromatography with Mass Spectrometric detection (GC–MS), and proteomics by Liquid Chromatography Mass Spectrometry (LC–MS/MS).

The marbles curated in Copenhagen are particularly interesting because these pieces have been kept indoors since before the onset of the industrial revolution in the 1700's. The sculptures remaining on the Parthenon for several centuries have experienced air pollution to a much larger degree.

Materials

Five samples were sequestered from the rear side of the head (National Museum No. ABb13, see Fig. 1 and 2). Milligram-size samples of substantially less than a square millimetre area was removed by a conservator using a hammer and chisel in September 1999. At locations P1, P2, and P3 the samples were typical of the brown stain. At sample location P4 the marble had a white, polished, slightly translucent lustre. Sample location P5 had an opaque white texture.

Experimental procedures

SEM–EDX analysis

The sample subjected to optical microscopy, SEM–EDX and LA-ICP-MS a subsample of KLR-2369/P2 were mounted perpendicular to the surface direction and embedded in Struers Epoxy resin. The sample was then polished to 1 μm diamond finish.

The Scanning Electron imaging and energy dispersive X-ray analyses (SEM–EDX) were performed with a Tescan Vega 3, using 20 kV accelerating voltage, a beam Intensity of 15, and a working distance of 15 mm. The machine was operating in Univac mode at a pressure of ca. 4 Pa taking the backscattered electron image. The EDX data was generated from an Oxford Instruments X-Max 20 mm^2 detector.
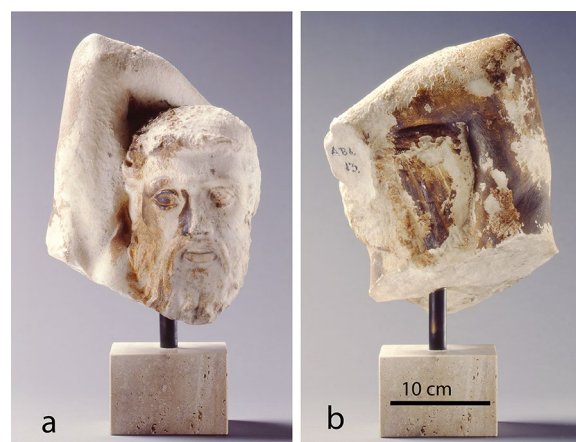

Fig. 1 The Centaur head at the National Museum in Copenhagen. **a**: front view; **b**: rear view. The brown stains are clearly visible. Courtesy of The National Museum of Denmark
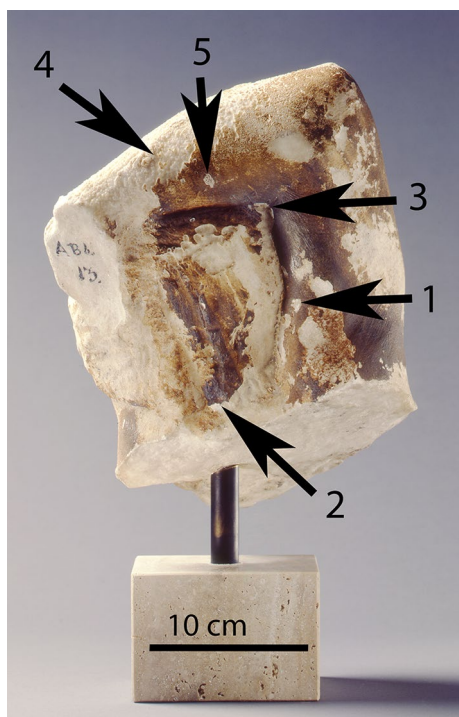
Fig. 2 Arrows show the sampling sites on the rear of the Centaur head

LA-ICP-MS analysis

Laser Ablation was performed with a CETAC LXS-213 G2 equipped with a NdYAG laser operating at the fifth harmonic at the wavelength of 213 nm. A circular aperture of 50 μm was used, and the shot frequency was 20 Hz. The line was scanned at 10 μm s^{-1}, taking 170 s to complete. The helium flow was 600 mL min^{-1}. Laser operations were controlled by DigiLaz G2 software provided by CETAC.

The ICP-MS analyses were undertaken with a Bruker Aurora M90. The radiofrequency power was 1.30 kW, plasma Ar gas flowrate was 16.5 L min^{-1}, auxiliary gas flowrate was 1.65 L min^{-1}, and sheath gas flowrate was 0.18 L min^{-1}. The following isotopes were measured without skimmer gas: ^{23}Na, ^{27}Al, ^{31}P, ^{44}Ca, ^{49}Ti, ^{52}Cr, ^{55}Mn, ^{57}Fe, ^{65}Cu, ^{66}Zn, ^{75}As, ^{88}Sr, ^{118}Sn, ^{121}Sb, ^{208}Pb, ^{232}Th, and ^{238}U. The analysis mode used was peak hopping using 3 points per peak. Isotopic interferences were corrected for by the ICP-MS software. The dwell time on each peak was 1 ms, expect for Na and Ca where the dwell time was reduced to 0.1 ms to avoid overflow in the counter. The measurements were preceded by a 10 s gas blank, the count rates of which were subtracted from the isotope count rates.

The quantification was performed by first adjusting the count rate for the isotopic abundance for the analysed isotopes. Following that the shape of the count rate as a function of atomic number was determined by analysing seven elements in a 5 ppb multi-element standard solution (XXI for MS, by Accustandard [30]). The isotopes used were: ^{9}Be, ^{25}Mg, ^{59}Co, ^{115}In, ^{140}Ce, ^{206}Pb, and ^{232}Th. The expected count rate in a 5 ng g^{-1} solution of the isotopes analysed for in this study was then calculated by interpolation between the measured count rates of these seven isotopes. Finally, the conversion from count rate to g g^{-1} was done by multiplying by a fixed ratio, determined by taking the average of the measurements in the marble zone and there fixing the average Ca concentration to 40 wt%. The brown stained layers were softer and easier to ablate, so here another calibration was needed, using an average Ca concentration fixed to 27 wt%. Due to possible deviations from the ideal stoichiometric compositions the data produced should likely be considered semi-quantitative rather than fully quantitative. Further details of the LA-ICP-MS methodology have been published elsewhere [30–33].

Micro X-Ray diffraction

The analysis was performed using a PANalytical X'Pert PRO MPD system (PW3050/60) with Cu Kα radiation as the source (λ = 1.54 Å) and a PIXcel1D detector. The X-ray generator was set to an acceleration voltage of 45 kV and the filament emission current to 40 mA. The divergence slit and the programmable anti-scatter slit were fixed at 0.5°. The capillary sample holder was mounted in an HTK 1200N Capillary Extension (Anton Paar) with a ceramic anti-scatter shield. The sample was scanned between 3° and 90° (2θ) with a counting time of 1700s, while the capillary was spinning around its own axis. Data were collected using X'Pert Data Collector. The data analysis was performed using Highscore Plus software and Crystal Impact Match software. Semi-quantitative concentrations have been acquired with the standardless reference intensity ratio method (RIR) [34] included in the Highscore Plus software using the I/Ic values from the ICDD PDF-2 and updated COD databases. These results provide the relative mineral abundance in the bulk sample assuming a 100% crystalline matrix.

After crushing and μ-XRD analysis the four samples (KLR-2368/P1, KLR-2369/P2, KLR-2370/P3, and KLR-2371/P4) were subjected to GC–MS in Pisa and LC–MS/MS in Odense.

GC–MS

Samples were subject to an analytical procedure that allows the separation of two different fractions, one for the analysis of amino acids, obtained from the acidic hydrolysis of proteinaceous matter, and another for the

Rasmussen *et al. Heritage Science*   (2024) 12:18

Page 6 of 17

analysis of the products of alkaline hydrolysis and organic solvent extraction of terpenoid and lipid materials. Blank analyses were routinely carried out and calibration curves were obtained, to determine the limit of detection (LOD) and limit of quantitation (LOQ), for both amino acids (amino acid fraction) and mono and dicarboxylic aliphatic acids (lipid fraction). For the analyses a gas chromatograph (6850N-Network GC system Agilent Technologies, Palo Alto, CA, USA) equipped with PTV injection port and coupled with a mass detector 5975C VL MSD (Agilent Technologies, Palo Alto, CA, USA) with a quadrupole analyzer was used. GC separation was performed on a fused silica capillary column coated with HP-5MS (J&W Scientific, Agilent Technologies; stationary phase 5% diphenyl–95% dimethylpolysiloxane, 30 m, 0.25 mm inner diameter, 0.25 μm film thickness) connected to a deactivated fused silica pre-column (J&W Scientific, Agilent Technologies; 2 m, 0.32 mm inner diameter). The details of the analytical procedure and the instrumental conditions are reported elsewhere [35].

Protein extraction and proteolytic digestion

Proteins were solubilized from 1 mg of the corresponding sample by the addition of 90 μL buffer containing 100 mM ethylenediaminetetraacetic acid disodium salt (Na_2EDTA), 2 M guanidine-hydrochloride, 150 mM triethylammonium bicarbonate (TEAB), 10 mM tris(2-carboxyethyl)phosphine hydrochloride (TCEP), and 20 mM chloroacetamide. The solution was set to react for 60 min at 56 °C in a vortex shaker to allow for efficient denaturing of proteins with reduction and alkylation of cysteine thiols. Following dilution of the solution to 1 M guanidine-hydrochloride by addition of 150 mM TEAB, proteins were digested with trypsin (1 μg) overnight at 37 °C. Digestion was terminated by acidification with 1 μL trifluoroacetic acid (TFA) and purified by desalting with tip-column reverse-phase chromatography. The purified sample was dried in a SpeedVac concentrator and stored at –20 C until LC–MS/MS analysis.

The blank control sample consisted of the protein solubilization buffer/enzyme and was processed using the same protocol (further referenced as *negative*).

Liquid chromatography and mass spectrometry analysis

Prior to injection, the sample was dissolved in 0.1% formic acid (FA). The analysis was executed using a Q-Exactive HF Mass Spectrometer (Thermo Fisher) coupled through a Nanospray Flex ion source (Thermo Fisher) to an Ultimate 3000 nano RPLC system (Dionex). Peptides were separated on a newly prepared fused silica column with an integrated emitter (25 cm×75 μm inner diameter) home packed with 2 μm Inertsil ODS-3 (GL Sciences) beads. The following solutions were used for LC separation: A–0.1% FA in water, B–0.1% FA in 95% acetonitrile. Samples were initially loaded on column with 2% B at a flow rate of 300 nL min^{-1}, the loading volume was 12 μL. The sample was eluted using the following gradient: in 1 min linear increase to 4% B, in 38 min linear increase to 30% B, in 6 min linear increase to 45% B, in 6 min linear increase to 95% B. The column was washed for 3.5 min with 95% B and equilibrated for the next injection at 2% B for 12 min. The flow rate was set to 300 nL min^{-1}. The mass spectrometer was operated in data-dependent mode; MS1 parameters: Resolution–120000 @ *m/z* 200, AGC target–3e6, Maximum injection time–50 ms, Scan Range–*m/z* 350–1400; MS^2 parameters: Resolution–60000 @ *m/z* 200, AGC target–2e5, Maximum injection time–125 ms. Up to seven precursors (Top 7) with charges from 2 to 6 (both included) were isolated in quadrupole using 1.2 Th window and fragmented with higher-energy collisional dissociation at normalized collisional energy of 28. Fragmented precursors were dynamically excluded for 12 s. To control for any possible contamination of the column 1μL of 0.1% FA was injected with the same method (Blank) before and after samples.

Database searching

Protein sequences (only reviewed) were obtained from the Uniprot resource (accessed 13–14.05.2021) and assembled into four databases used for the analysis: 1) proteins belonging to bacteria (taxon: *Bacteria*, taxonomic id: 2, 334967 entries); 2) proteins belonging to vertebrates (taxon: *Chordata*, taxonomic id: 7711, 86255 entries); 3) proteins belonging to fungi (taxon: *Fungi*, taxonomic id: 4751, 35153 entries); 4) proteins belonging to higher plants (taxon: *Embryophyta*, taxonomic id: 3193, 39058 entries). Acquired LC–MS/MS files were analyzed in three steps. First, FragPipe 19.1 with MSFragger 3.7 and Philosopher 4.8.1 has been employed for open modification search and unspecific cleavage search. Open modification search parameters: precursor tolerance was –150–500 Da, MS^2 tolerance was 7 ppm, isotope error was 0, top 175 peaks per spectrum used for search, peptide length was 7–35 amino acids, peptide mass was 500–3500 Da, enzyme was trypsin without the proline rule, carboxamidomethylation of cysteine as fixed modification and oxidation of methionine and acetylation of protein N-terminus as possible variable ones, all other parameters were used as set in the open search template. Unspecific cleavage search parameters: precursor tolerance was 10 ppm, MS^2 tolerance was 10 ppm, isotope error was 0 or 1, top 200 peaks per spectrum used for search, peptide length was 7–25 amino acids, peptide mass was 500–3500 Da, no enzyme,

Rasmussen *et al. Heritage Science*   (2024) 12:18

Page 7 of 17

carboxamidomethylation of cysteine as fixed modification and oxidation of methionine as variable one, all other parameters were used as set in the default template.

Next, Proteome Discoverer 2.5 (Thermo Fisher Scientific) using MSAmanda 2.0.0.16129 was used to search against each database individually. The following search parameters were used: enzyme – semi trypsin, precursor tolerance was 5 ppm, fragment tolerance was 20 ppm, carboxamidomethylated cysteines were used as fixed modification, and oxidized methionine as variable modifications. Search results were validated using Percolator.

Finally, we identified all organisms with at least one reliably identified protein in the first two steps and extracted complete proteomes of these in a new database (79859 entries from 41 taxons). Proteome Discoverer was used for the search with the following variable modifications: oxidation of methionine, proline, and serine; deamidation of asparagine and glutamine; pyroglutamic acid formation from N-terminal glutamine. All other parameters were the same as for the second step. Proteins identified with a single peptide were filtered out. All peptides, including the shared ones were considered for judging protein presence in the samples.

Results

Optical microscopy

A subsample of KLR-2369/P2 was mounted perpendicular to the original surface and polished. In Fig. 3 optical microscopy images can be seen at three different magnifications. Two brown stained layers, each of ca. 50 μm thick, are visible at the top of Fig. 3a, followed by a layer appearing white in the polarized reflected light. Finally at the bottom of Fig. 3a is seen the marble substrate appearing grey in colour. Two Laser ablation tracks made with a beam diameter of 50 μm are slightly visible, as indicated by the two white arrows. At higher magnifications (Fig. 3a and b) is seen several red and dark brown grains of up to a few microns in size.

SEM–EDX

The same cross section of subsample of KLR-2369/P2 has been analysed by SEM–EDX. Twelve points have been analysed, three in the two brown stained layers (points 1, 2, and 3), the two brown stained layers are not distinguishable in the backscattered electrons picture, two
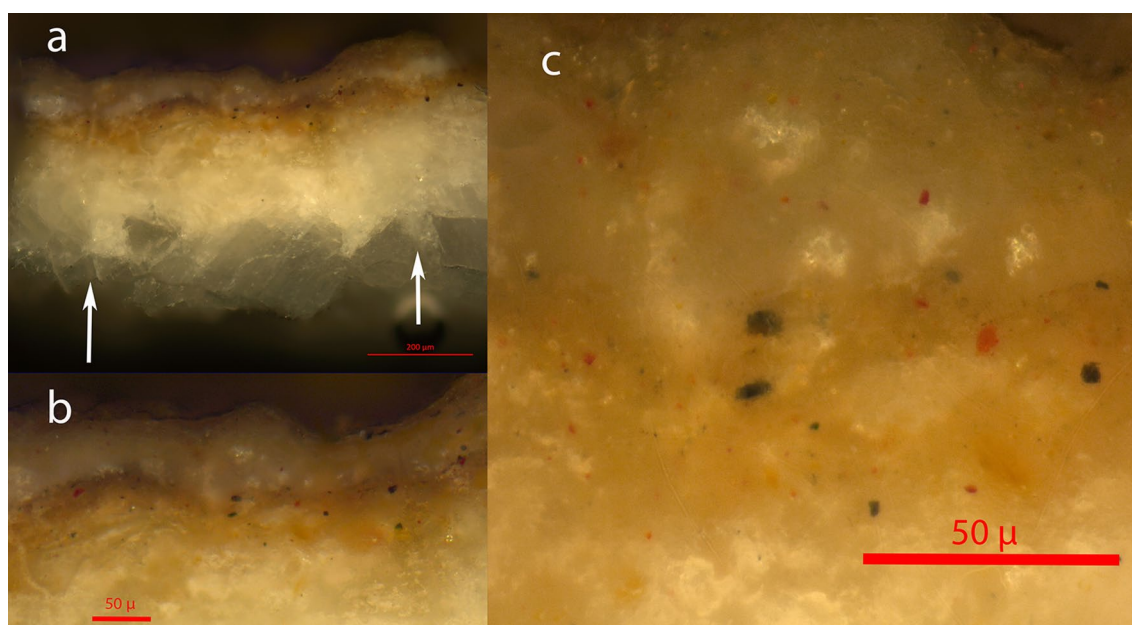

Fig. 3 Optical microscopy (OM). Photo in polarized light of a subsample of KLR-2369/P2 mounted edge-on–the surface being at the top of the pictures. **a**: Two brown stained layers, each of ca. 50 μm thick, are visible at the top; followed by a layer appearing white in the polarized reflected light; finally at the bottom the marble substrate appearing grey. Two Laser ablation tracks made with a beam diameter of 50 μm are slightly visible as indicated by two white arrows. **b**: magnified detail showing the two brown stained layers and featuring several red and dark brown grains of up to a few microns in size; **c**: further magnification showing a difference in size distribution of both the red and dark brown pigments

Rasmussen *et al. Heritage Science*   (2024) 12:18

Page 8 of 17

Table 1 Results of the SEM–EDX analyses of sample KLR-2369/P2

	Type	C Wt%	O Wt%	Na Wt%	Mg Wt%	Al Wt%	Si Wt%	P Wt%	S Wt%	Cl Wt%	K Wt%	Ca Wt%	Cr Wt%	Mn Wt%	Fe Wt%	Ni Wt%	Mo Wt%	Sum Wt%
Point 1	Brown	33.73	45.53	0.38	0.20	1.19	1.36	1.85	0.17	0.17	0.64	14.42	0.01	0.01	0.29	0.03		100
Point 2	Brown	32.80	46.36	0.19	0.25	1.58	1.84	0.97	0.12	0.19	0.55	14.79		0.02	0.33			100
Point 3	Brown	33.02	44.30	0.22	0.31	2.03	3.02	1.32	0.18	0.24	0.71	14.26	0.02	0.01	0.33		0.03	100
Point 4	White	29.47	44.18	0.48	0.71	0.99	0.37	7.12	0.50	0.53		15.51	0.01	0.02	0.07	0.03		100
Point 5	White	29.09	35.61	0.42	0.64	0.91	0.38	9.05	0.72	0.66		22.30		0.07	0.13	0.03		100
Point 6	Grey	28.21	32.32	0.15	0.44	1.03	0.32	5.87	0.51	0.50		30.36	0.01	0.11	0.19			100
Point 7	Grey	28.34	42.51	0.09	0.40	1.09	0.13	0.88	0.07	0.15		26.14		0.04	0.06			100
Point 8	Grey	28.35	43.33	0.08	0.51	1.10	0.10	0.61		0.14		25.59	0.01	0.00	0.03		0.16	100
	Avg brown	33.18	45.40	0.26	0.25	1.60	2.07	1.38	0.16	0.20	0.63	14.49	0.02	0.01	0.32	0.03	0.03	100
	Avg white	29.28	39.90	0.45	0.68	0.95	0.38	8.09	0.61	0.60		18.91	0.01	0.05	0.10	0.03		100
	Avg grey	28.30	39.39	0.11	0.45	1.07	0.18	2.45	0.29	0.26		27.36	0.01	0.05	0.09		0.13	100

The data have been summed to 100 wt%. Average composition of the brown stain, the white, and the grey zones as well as the average of the dark mineral grains are listed in the lowermost lines
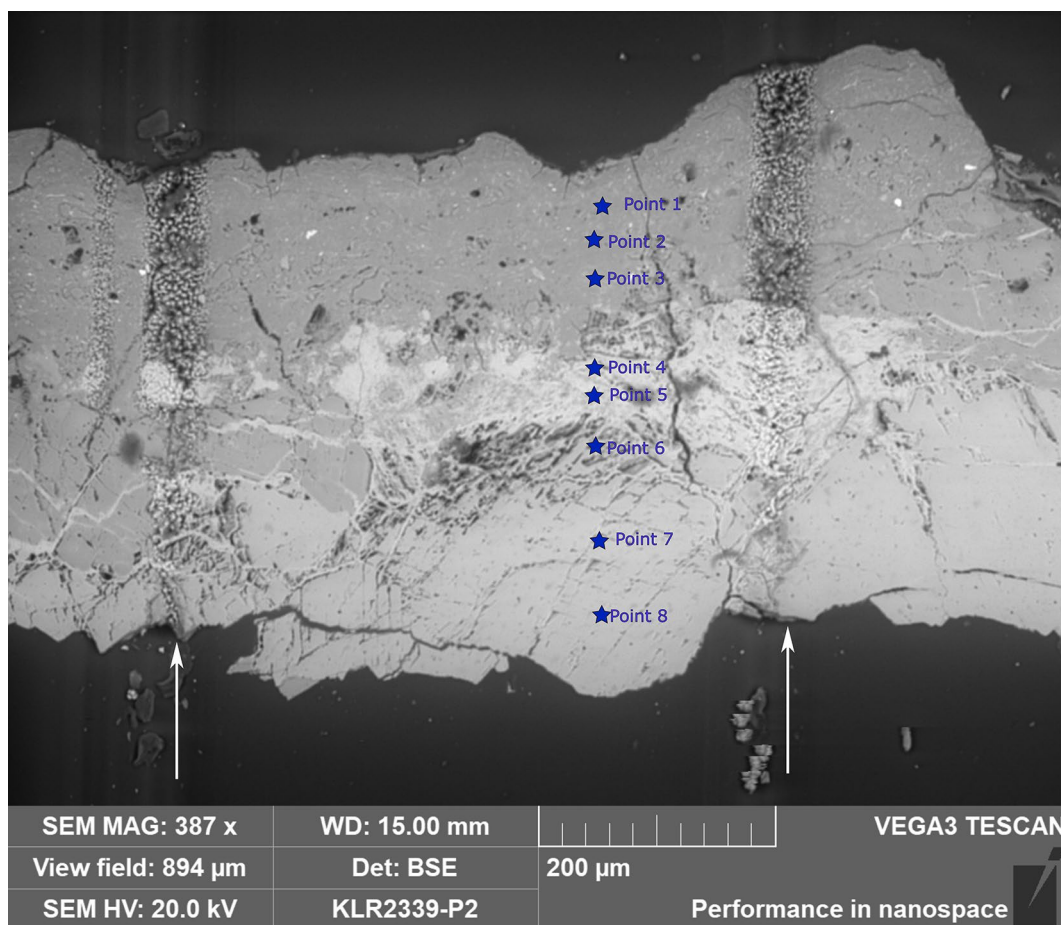

Fig. 4 Backscattered electron image from the SEM (BSE). Two Laser ablation tracks made with a beam diameter of 50 µm are visible are indicated by two white arrows. The ICP-MS data from the linear trace to the right is reported below

Rasmussen *et al. Heritage Science*   (2024) 12:18

Page 9 of 17

points in the white zone (points 4 and 5), three points in the grey substrate zone (points 6, 7, and 8). The data are listed in Table 1 and the position of the points are shown in Fig. 4.

µXRD

Another sub-sample of KLR-2369/P2 containing both the brown stain, white zone, and grey zone material was subjected to µXRD. The subsample was crushed and placed in a capillary tube, which was mounted on a rotational stage for the acquisition of the XRD pattern. The resulting diffractogram is shown in Fig. 5. The following phases were detected, and the semi-quantitative proportions have been determined by using the reference intensity ratio method (RIR): 63% calcite ($CaCO_3$), 23% whewellite ($CaC_2O_4 \cdot H_2O$), 5% weddellite ($CaC_2O_4 \cdot 2H_2O$), 4% gypsum ($CaSO_4 \cdot 2H_2O$), 3% iron oxide (Fe_3O_4), and 1% quartz (SiO_2). No clay minerals were seen in the diffractogram, nor any hydroxyapatite.

LA-ICP-MS

A trace made by a 50 µm diameter beam was analysed by LA-ICP-MS. The positions of the two traces are marked in Figs. 3 and 4. One trace was a test used for parameter optimization; the data of the other trace are shown in Fig. 6.

Organic material analyses

GC–MS analyses showed the presence of traces of monocarboxylic aliphatic acids (palmitic and stearic acids) with a profile that is not specific to any lipid materials, and which is compatible with environmental contamination. Amino acids were below the LOD of the analytical procedure. This result is not conclusive, though, as proteins are subject to significant changes over centuries of aging. Among these changes, aggregation, cross-linking, and formation of complexes with inorganic species resulting in a substantial loss of solubility, which may prevent the detection of proteins using GC–MS based analytical approaches [36–39].

LC–MS-based proteomics is a very sensitive analytical method, and it enables the routine detection of sub-nanogram quantities of individual proteins [40]. For this reason, the same samples which were analysed by GC–MS, were also analysed by LC–MS-based proteomics.

Our database search approach of LC–MS data employed three tiers allowing us to improve the sensitivity of the analysis by considering only relevant parameters, such as modifications and digestion specificity. We started our investigation with open-modification and unspecific database searches against four large databases containing proteins from bacteria, fungi, plants, and vertebrates. This approach accounts for potential partial degradation including any type of modification of the proteins even when the precise mechanism of such is not known. The results of these searches were used to refine the parameters of a traditional database search engine by choosing only a limited number of frequent variable modifications to be considered for the search against the
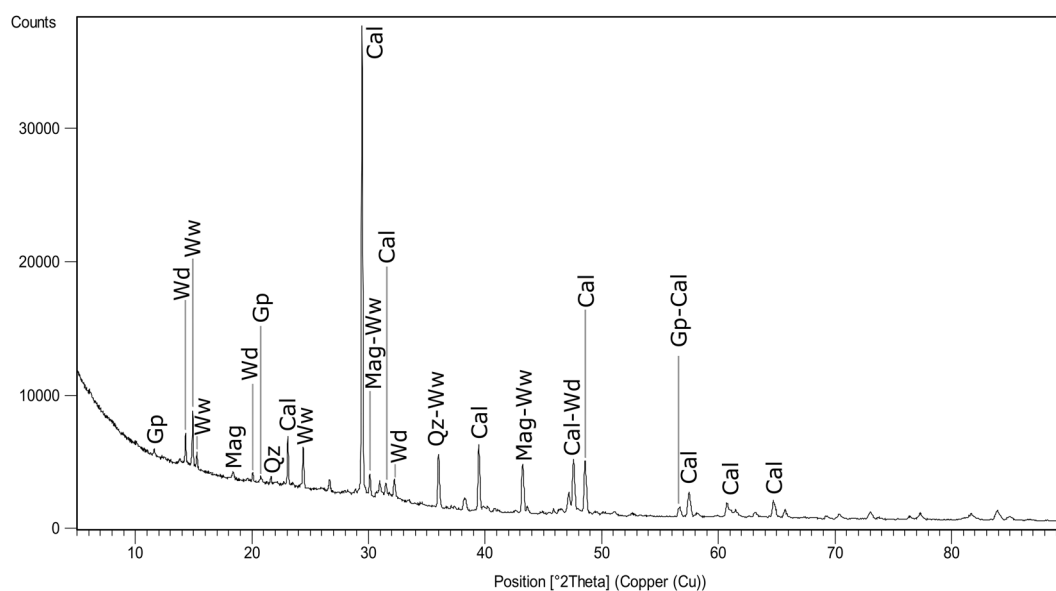

Fig. 5 XRD pattern of sample KLR-2369/P2. *Gp* gypsum ($CaSO_4 \cdot 2H_2O$), *Qz* quartz (SiO_2), *Cal* calcite ($CaCO_3$), *Wd* weddellite ($CaC_2O_4 \cdot 2H_2O$), *Ww* whewellite ($CaC_2O_4 \cdot H_2O$), *Mag* magnetite (Fe_3O_4)

Rasmussen *et al. Heritage Science*   (2024) 12:18
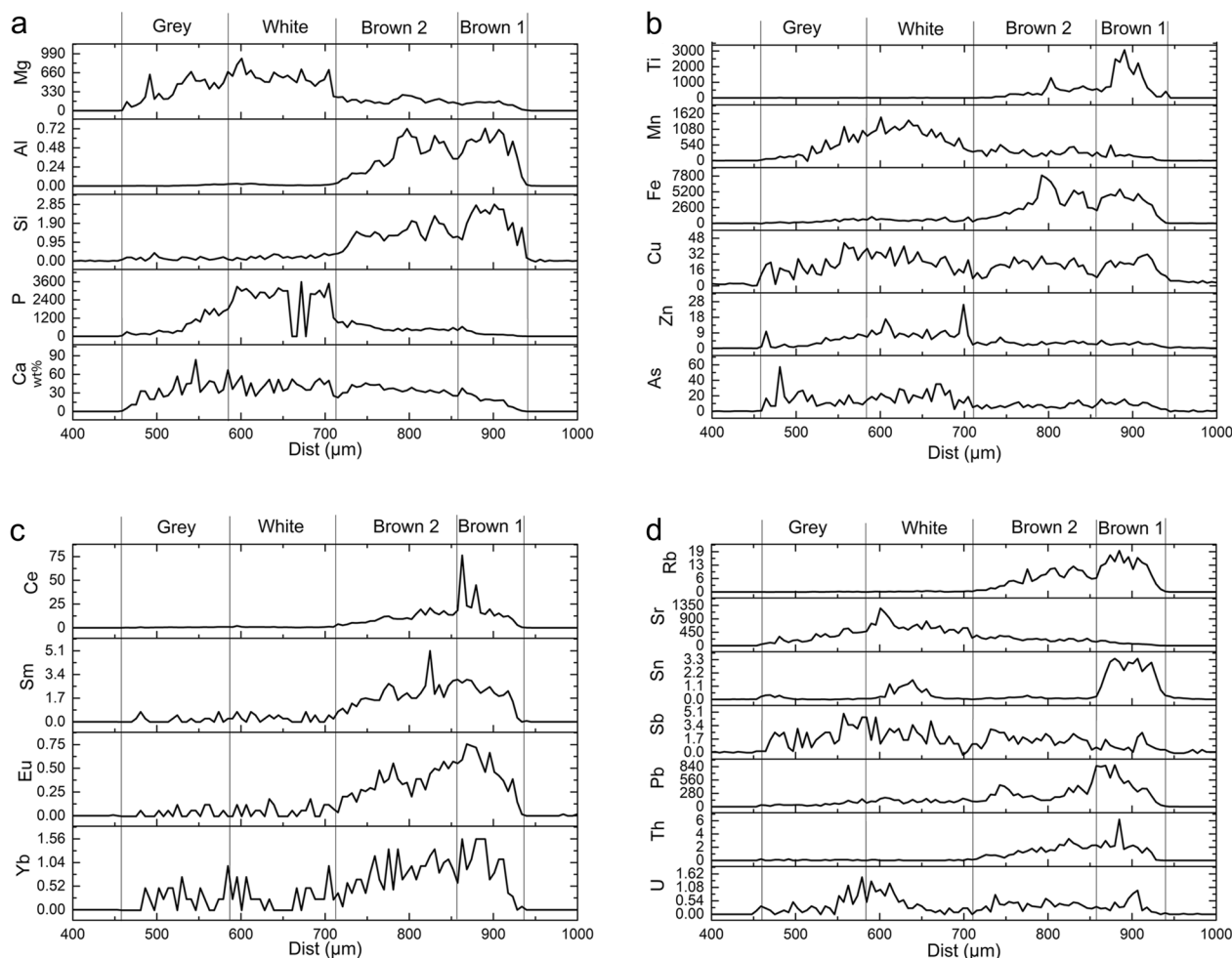
Page 10 of 17

Fig. 6 a, **b**, **c**, and **d**: Calibrated LA-ICP-MS elemental concentrations in a 10 μm wide line perpendicular to the surface of sample KLR-2369/P2. Calcium is shown in wt%, while the rest is given in μg g^{-1}

same databases. Finally, we used organisms identified in the previous two steps to create a new smaller mixed species database and performed the search using a much larger list of protein modifications, commonly reported in ancient samples.

Open-modification search allows undefined (wildcard) modifications to be included as part of the identified peptides. An unspecific cleavage database search makes no assumptions regarding the enzymatic process by which peptides are formed from protein in the sample.

During the open modification search, only the search against the vertebrate protein database was able to provide reliable peptide identifications. All the detected modifications were infrequent (less than 10% of all identifications in the corresponding sample), thus, we can conclude the proteins in the studied samples had no ubiquitous modifications, which must be accounted for during the following analysis. In doing so we aim to

balance computational efficiency, statistical rigor, and biological relevance, ultimately leading to more accurate, sensitive, and reliable protein identifications.

The unspecific search against the vertebrate database indicated a significant number of semi-tryptic peptides, *i.e.*, the peptides that have one terminus that has not been formed by the action of the digestion protease, thus, we used semi-trypsin as the enzyme for the later search stages. The unspecific search against the bacteria databases did not return any confident identifications. In the second search, no positive identifications can be made from bacterial, fungal, and plant databases. The final search against the mixed species database led to the identification of a total of 77 proteins in all analysed samples. However, only 17 of them were not detected in the negative control sample and therefore cannot be explained as a result of the sample preparation. Among these proteins, three belong to the keratin class of proteins. Keratins are

Rasmussen *et al. Heritage Science*   (2024) 12:18

Page 11 of 17

Table 2 Proteins identified in samples during the last database search (against the refined multi-organism database)

UniprotID	Protein name (origin)	Number of identified peptides	Negative (preblank)	Negative	P1 (preblank)	P1	P2 (preblank)	P2	P3 (preblank)	P3	P4 (preblank)	P4	P5 (preblank)	P5
P02768	Albumin (primate)	2	×	×	×	✓	×	×	×	×	×	✓	×	×
P0DUB6	Alpha-amylase (mammalian)	3	×	×	×	×	×	×	×	×	×	✓	×	✓
P00690	Alpha-amylase (mammalian)	3	×	×	×	×	×	×	×	×	×	✓	×	✓
P28814	Barwin (cereal plants)	2	×	×	×	△	×	△	✓	△	△	△	△	✓
Q5R1M5	Chymotrypsin-like elastase 1 (mammalian)	2	×	×	×	△	△	×	×	×	×	×	△	✓
Q9UNI1	Chymotrypsin-like elastase 1 (mammalian)	5	×	×	×	△	△	×	×	△	×	×	△	✓
P08217	Chymotrypsin-like elastase 2 (mammalian)	2	△	×	×	×	×	×	×	×	×	×	×	✓
Q91X79	Chymotrypsin-like elastase 1 (mammalian)	4	×	×	×	△	△	×	×	△	×	×	△	✓
P00773	Chymotrypsin-like elastase 1 (mammalian)	3	×	×	×	△	△	×	×	△	×	×	△	✓
P02453	Collagen alpha-1 (vertebrate)	7	×	×	×	✓	×	✓	×	△	×	✓	△	✓
P02465	Collagen alpha-2 (vertebrate)	5	×	×	×	✓	×	△	△	△	×	✓	△	✓
C0HJP0	Collagen alpha-2 (vertebrate)	3	×	×	×	×	×	✓	△	×	×	✓	×	✓
Q4A3R3	Hensin (mammalian)	2	△	×	×	×	×	×	×	△	×	△	×	✓
P02845	Vitellogenin-2 (avian)	2	×	×	×	×	△	×	△	△	×	✓	×	△

Symbols: × – not observed; △ – observed, by identification transfer; ✓ – observed and identified. Identification transfer is a technique used in analysis of the related samples, when a peptide identified in one sample is transferred to another sample using its retention time and mass; *pre-blank* stands for the 0.1% FA injection immediately before the sample analysis (contamination control)

known to be a common contaminant introduced during sample handling [41]. The remaining 14 proteins are presented in Table 2. It should be noted that none of the detected proteins were specific for the brown stain regions (P1, P2, P3) only.

All detected proteins can be organized into seven classes: albumin, vitellogenin, chymotrypsin-like elastase, alpha-amylase, collagen, barwin, and hensin. Due to the nature of the LC–MS/MS analysis we employed, we can only detect peptides, which are partial sequences of proteins. Therefore, it is crucial to account for other potential origins for these peptide sequences. To address this, we have used BLAST [42]. This is done by comparing the peptide sequences against a database containing sequences of other species to infer if these peptides are unique to one species or part of homologous sequences shared by many organisms.

Two peptide sequences initially assigned to human albumin are shared with albumins of several other primates, although the similarity to albumins from common domestic animals, such as pigs and cows, is so insignificant that these origins can be excluded. Two peptides assigned to vitellogenin are shared with vitellogenins and phosvitins from several avian species and hence cannot be assigned with absolute certainty (Additional file 1 contains BLAST results for the peptide sequences, only proteins with the complete identity listed). Peptides detected for alpha-amylase, chymotrypsin-like elastase, and collagen groups are shared between many mammalian species, including domestic animals and pests, humans, and wild animals; thus, precise identification of the origin cannot be determined. Detected peptides of barwin could also be explained by related proteins from other cereals, they belong to the so-called barwin-like domain, reported in several cereal plants, such as barley, wheat, goatgrass, and wild einkorn. Peptides assigned for hensin correspond to the scavenger receptor cysteine-rich domain part of that protein and are shared with a number of other mammalians, such as rabbits, felines, and rodents; a human origin is, however, unlikely.

Albumin is a major protein found in animal blood. Therefore, its presence in the sample is most likely due to contamination during the handling of the artifact by humans. Since the detected peptides are not commonly found in domestic animal albumins, it is unlikely that the artifact has been treated with any blood-containing animal product. Vitellogenin-2 is the major protein of egg yolk, which is known to be used as a paint binder, and thus one can speculate that the source could be a paint applied to the artefact. Alpha-amylases and elastases are found in saliva and pancreatic fluids of mammals, including humans, thus, the possible explanation is contamination during handling where small droplets of saliva

aerosols can have been deposited on the material or contamination by excretions of domestic animals or pests. Collagens are typical proteins found in animal connective tissues, including ligaments, tendons, and bones. These proteins are the main component of animal glue, and, thus, its presence in virtually all samples can be explained by treatment during production or later conservation of the piece of art (although we do not have any indication that conservation has ever been attempted). Due to the high similarity of animal collagens, the source of collagen in the samples remains ambiguous. As expected for collagens, most of the detected peptides are identified as having hydroxyproline residues and, thus, were detected only in the final search. Barwin-like proteins were reported to be a part of plant defence against pathogens and accumulated during seed maturation. The presence of this protein could be due to the treatment of the marble with some cereal-based product, such as flour, or environmental contamination. Proteins having scavenger receptor cysteine-rich domain (as detected in hensin) are observed, among others, in saliva and intestine as a part of the innate immunity system, thus, similarly to alpha-amylase, their detection is likely due to contamination by some biofluids of domestic animals and pests.

All detected proteins have been confidently detected with at least two statistically significant peptides. In comparison to our routine analysis, these peptides were found to have lower intensity but were still well within the detection range. Therefore, we estimate the protein quantities to be in the upper-picogram range. The supplementary material contains annotated spectra for all peptides and proteins detected in the experiment (see Additional file 2). Each spectrum is supplemented with MS2PIP prediction [43] for the same sequence.

Discussion

The optical microscopy pictures show two superposed surficial brown stained layers of almost similar thickness each approximately 50 μm thick (Fig. 3a). The two brown stained layers can be viewed in detail in Fig. 3a and b. Both layers feature several red and black/dark-brown grains with a wide size distribution of both the red and dark brown grains (Fig. 3c). Below the brown stain is seen a layer appearing white in both optical microscopy (OM) and backscattered electron image (BSE) (Figs. 3a and 4). The white layer has a varying thickness and a filament-like appearance, but with an overall average thickness of approximately 50 μm. The white layer is somewhat enriched in P compared to the other layers. Below this can be seen the substrate layer which appears greyish in both the OM and BSE images, and which most likely consists of marble (Figs. 3a and 4). These layers will be discussed in further detail below.

The grey substrate

The average elemental composition of the grey zone as analysed by SEM–EDX can be seen in the lowermost rows of Table 1 while the low mass elements of the LA-ICP-MS data can be seen in Figs. 6 and 7. Figure 7 also shows elemental mappings of Al, Si, P, Ca, and Fe. Calcium and Mg are higher in the grey zone compared to the brown stain. Furthermore, the grey substrate zone is enriched in Mg, Mn, Sr, and Sb relative to the brown stain as can be seen in the LA-ICP-MS data (Fig. 6). Taking the results of the µXRD pattern into consideration and the general fact that the figure head is made of marble, it appears that the grey zone is indeed the marble substrate and that it consists of relatively pure calcite with minor amounts of gypsum (0.29 wt% S on average, according to the SEM–EDX, see Table 1).

The white zone

The white zone is higher in P compared to the brown stained zone and the grey substrate zone, ca. 8.1 wt% on average according to the SEM–EDX data (Table 1). However, no P-containing minerals like *e.g.,* hydroxyapatite, were identified in the XRD pattern, which could possibly be due to a haphazard lack of white zone material in the small sample exposed to capillary µXRD. Also, there is a discrepancy between the not so high P concentrations determined by LA-ICP-MS (a maximum of ca. 0.3 wt%) and the higher P-concentration determined by SEM–EDX (8.1 wt%), This could possibly be due to inhomogeneities and therefore potential differences in the sample materials analysed by the two methods. It can be speculated that the material in the white zone is merely slightly altered marble. It could also be a vein of P-richer material in the original marble. Finally, there is the possibility

that the white zone originates from the application of a conservation or restauration treatment despite the fact that no P-bearing phase (e.g., hydroxyapatite, brushite) was identified in the XRD pattern. The use of phosphate-based materials such as diammonium hydrogen phosphate (DAP) has been recently studied (*e.g.,* [44, 45]), but the absence of records for modern restoration campaigns and the position of the white layer below the two brown stained film layers would a priori discard the hypothesis of a modern treatment since these sorts of stains have been observed at least since the early eighteenth century. However, the possibility of an old and unrecorded restoration treatment is possible, although very unlikely. During the nineteenth century, several conservation methods were employed to consolidate and restore heritage buildings [46]. While the application of fluorosilicate following the Kessler's method can be dismissed in our case considering the absence of fluorine detected by the SEM–EDS analysis, the Ransom's method patented in 1856 can be considered [47]. The Ransom's method includes the application of three successive layers of calcium phosphate, barite solution, and alkaline silicate. While the white layer shows a higher amount of P, there is no increase in the Si content and no trace of Ba is detected. Based on the results of SEM–EDS data, hydroxyapatite remain the only conservation material matching the elemental composition measured. Moreover, it should be noted that the Ca:P ratio observed in the SEM–EDS results ranged between 2.1 and 2.4, which could match the expected value for hydroxyapatite in bones considering deviations from the stoichiometric ratio which could originate from various factors and processes [48]. However, because of the absence of identified phases in the µXRD results, these observations leave the precise
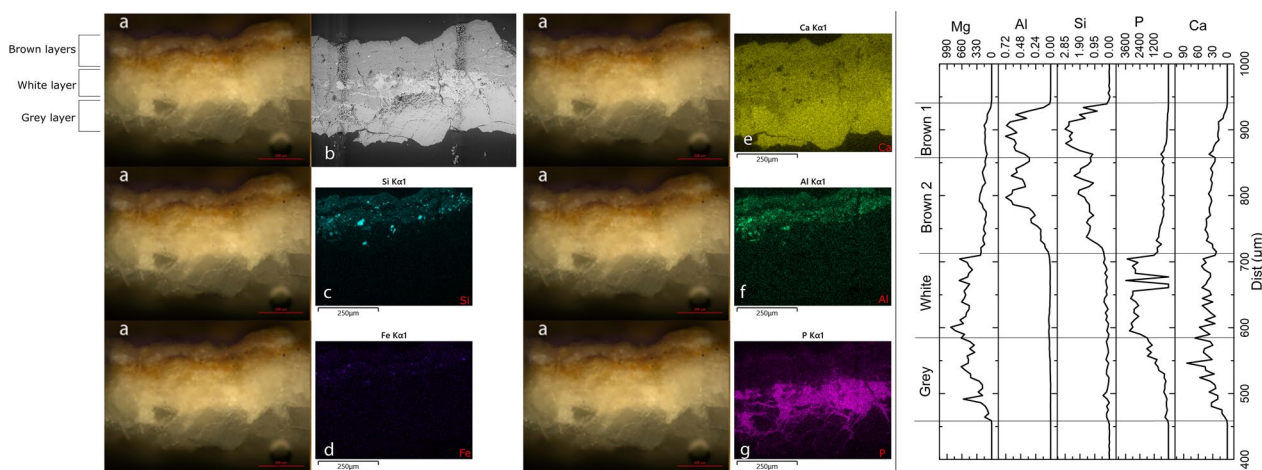

Fig. 7 Comparison of the OM image (**a**) with the BSE image (**b**), and the SEM–EDX elementary mappings of Si (**c**); Fe (**d**); Ca (**e**); Al (**f**); and P (**g**). To the right a cross section of the low mass elements measured by LA-ICP-MS for further comparison

Rasmussen *et al. Heritage Science*   (2024) 12:18

Page 14 of 17

mineralogical composition of the white zone unsolved in the present study.

The two brown stained film layers

The presence of the two oxalate phases whewellite and weddellite, which sum up to as much as 28 wt% of the composite sample subjected to µXRD, makes it safe to conclude that the brown stained layers mainly consist of Ca-oxalates. This is supported by the SEM–EDS and LA-ICP-MS results show that the two brown stained film layers are made of a Ca-rich matrix with higher values for Al, Si, and Fe compared to the marble background. The presence of quartz, iron oxides, and the two oxalate phases whewellite and weddellite seen in the XRD pattern is somewhat in agreement with the elemental characterisations. However, no aluminium-bearing minerals were identified in the XRD-pattern, which could be caused by inhomogeneity or haphazard lack of these minerals in the small sample exposed to capillary µXRD.

The presence of two distinct brown layers, or films, can be seen both in the OM pictures (Fig. 3) and in the LA-ICP-MS profiles for Al, Si, Fe, Co, Cu, Tl, Pb, and REE (Fig. 6). The fact that the two brown stained layers are so distinct from each other speaks against a migration of materials from inside the marble, and likely also rules out a reaction of the marble surface with the environment via for instance a hypothetical air-chemistry process. A conservation treatment cannot be excluded, however, nor can a deliberate original treatment in connection with the creation of the piece of art.

The average content of S in the brown zone as measured by SEM–EDX is 0.16 wt% (Table 1). This very low number counter-indicates that the brown stain layers were formed as a result of atmospheric deposition of oxalates, *e.g.,* from fossil fuel combustion processes, as these are often combined with SO_2-rich air pollution [49, 50]. A modern air pollution formation is also unlikely for another reason also, namely that the head of the Centaur has been kept indoors since before the onset of the industrial revolution. The low level of S can to some extent be viewed as conforming with a hypothesis of a biological origin, as for example algae or lichen, because these are sensitive to the occurrence of S-containing compounds [51, 52].

What concerns the enrichment of Al and Si the likely explanation is the presence of these elements in small particles embedded in the oxalate phases. The XRD pattern revealed the presence of quartz, which can explain the enrichment of Si, while no phases were identified containing Al, although such minor phases could be overlooked in the µXRD experiment due to the small sample size and none-random grain size orientation in the capillary.

An interesting difference is seen between the chemical composition of the outer and inner oxalate layer in terms of the concentrations of Ti and Sn, and to some degree also Rb and Pb (Fig. 6). Titanium and Sn occur in some abundance in the outer oxalate layer (ca. 3 µg g^{-1} for Sn and ca. 2500 µg g^{-1} for Ti), but Sn is almost absent from the inner oxalate layer and the Ti concentration is a factor of five less in the inner oxalate layer compared to the outer. For Rb, the concentration in the outer layer is approximately double of that in the inner layer, and the same goes for Pb. Contrary to this, Al, Si, Fe, and Cu are present in similar amounts in the two layers. The distinct differences in the trace element concentrations in the two brown layers points towards a different origin of the two layers, at least temporally.

To summarize the entire data set, it seems likely that the grey substrate layer is the original marble, while the origin of the white zone remains unclear. The two brown-stained surficial layers of almost similar thickness consist of the calcium oxalate minerals weddellite and whewellite, which theoretically could be decay products from two now unidentifiable organic phases – either the excretion of oxalic acid from a biological organism growing on the marble or the organic binder from two consecutive paint layers, normally containing albumin, bone collagen, casein, or polysaccharides [53]. The use of egg as a binding agent in paint has been recorded since ancient times, evident in artworks from the Mediterranean region dating back to the Bronze Age [54–57]. This practice extended to polychrome artifacts found not only in the Mediterranean Sea area [58], but also in regions as far-reaching as China, with connections to the Silk Road [59–63]. Milk used as a paint binder in the ancient world is not as extensively documented [59]. However, it was identified in the Buddhas of Bamiyan (Afghanistan, 7th Century CE), likely used in both the original artwork and subsequent historical restoration layers [64].

However, the results from the proteomics do not support this. Embedded in the oxalates are two coloured phases, a black phase which could be magnetite, and a red phase which is possibly maghemite or hematite. The grain sizes for these two colorant phases are typically a few µm or less.

With the distinct exception of the different trace element chemistry inventory of Ti, Sn, Rb, and Pb in the two oxalate layers, many of the other features observed here, have previously been described in the literature ([24, 65], see also the comprehensive review by Rampazzi 2019 [29] and references therein). However, it was one of the aims of the present work to investigate if the calcium oxalates contain any organic progenitor or decay product, which could give an indication of a possible biological origin and, if so, the organisms responsible for its formation,

Rasmussen *et al. Heritage Science*   (2024) 12:18

Page 15 of 17

e.g., fungi, lichens, algae, or cyanobacteria, which has previously been suggested [66–70]. The proteomics analysis was able to reveal several proteins from humans, other mammals, birds, and plants, none of them, however, was specific to the stained regions. Thus, they are relevant to the object as a whole, but cannot explain the formation of the brown stain. There is a very small possibility that currently unsequenced proteins (and, thus, not present in genetic or protein databases) were not detected in our study. The list of sequenced species, however, includes most common domestic animals, including, cattle, birds, and fish, and, thus, the presence of any products derived from them seems highly unlikely. Furthermore, it is well-established that proteins from closely related species exhibit significant sequence similarity, resulting in similar protein structures. As a result, we anticipated the presence of many identical peptides during the LC–MS proteomics analysis. By utilizing comprehensive database searches as described above, we can effectively encompass a wide range of potential biological sources, even if the exact organism of origin is not explicitly represented in the database.

This study did also consider the possibility of partial degradation of the proteins in the sample by employing open modification and unspecific search, which allow the detection of unexpected protein modifications and non-enzymatic degradation products, respectively. The employed method (bottom-up proteomics) still relies on protein sequence databases, and hence if proteins were heavily modified or degraded it might be impossible to reliably identify them.

The absence of commonly detected biological progenitor molecules in the five samples of the Centaur head is not direct evidence against a biological origin, but it does significantly lower the likelihood of a biological origin.

Conclusions

A brown stain discernible with the naked eye is present on the Centaur head curated in Denmark. Five small samples from the head have been sequestered and analysed in this study. Optical microscopy revealed that two visually distinct brown surficial layers are present, one on top of the other and with approximately equal thickness. It has been established that two types of coloured grains, one dark brown and one red both homogeneously embedded in two superposed brown stained films consisting of whewellite and weddellite. Based on the XRD pattern some of the particles are interpreted to consist of iron oxide. Even though only quartz and iron oxide were identified in the XRD pattern, it is likely that both Al and Si are situated in grains embedded in the oxalate phases. The two brown layers are distinctly different in their trace element concentrations of Ti, Rb,

Sn, and Pb. It is therefore likely that the two brown layers have different origins, at least timewise. It can also be concluded that no diffusion process, re-crystallization process, or mechanical alteration process have taken place in the two layers. It cannot be ascertained from the present work if the two layers were part of paint layers, the result of a later painting, or conservational treatments.

Several proteins from humans, other mammals, and plants were detected and could be ascribed to human or environmental contamination. Detected vitellogenin-2, an egg yolk protein, and animal collagens could possibly be related to a hypothetical binder of a degraded paint layer and animal glue, respectively, hypothetically employed during the production of the piece of art or by past conservational treatments, *e.g.,* a production of plaster casts. However, both can also be explained by environmental contamination. Despite a thorough search, no organic compounds were found specific to the brown stained areas. So, although a biological origin of the brown stained layers cannot be completely excluded because of the possible complete degradation of *e.g.*, past paint layers or hypothetical conservational treatments, the inhomogeneous trace element distributions of the brown film still remain interesting and unexplained.

Rasmussen *et al. Heritage Science*   (2024) 12:18

Page 16 of 17

Declarations

Author details
[1]Cultural Heritage and Archaeometric Research Team (CHART), Department of Physics, Chemistry and Pharmacy, University of Southern Denmark, Campusvej 55, 5230 Odense M, Denmark. [2]Formerly, Department of Classical Antiquity, National Museum of Denmark, Frederiksholms Kanal 12, 1220 Copenhagen, Denmark. [3]Cranfield Forensic Institute, Defence Academy of the UK, Cranfield University, Shrivenham SN6 8LA, UK. [4]Dipartimento di Chimica e Chimica Industriale, Pisa University, Via Moruzzi 13, 56124 Pisa, Italia. [5]Department of Biochemistry and Molecular Biology, University of Southern Denmark, 5230 Odense M, Denmark.

References
1. Jacobaeus H. 1696. The Royal Museum Museum Regium. Hafniae; Copenhagen
2. Rumohr KFv. (in German) Antiquities and treasures of art in Copenhagen and in Zealand in general. Alterthümer und Schätze der Kunst zu Kopenhagen und in Seeland überhaupt. Kunstblatt, Nr. 88, 3. November. 1825.
3. Rasmsussen BB. London in reality the capital of Europe. PO Brøndsted's dealings with the British Museum. In: Rasmussen BB, Jensen JS, Lund J, Märcher M, editors. A Danish Classicist in his European Context. The Royal Danish Academy of Science and Letters. Copenhagen. 2008
4. Brøndsted PO. Travels and investigations in Greece: along with a presentation and explanation of many newly discovered Greek-style monuments, and a critical overview of all of Pausanias's undertakings of this type up to our own times. Reisen und Untersuchungen in Griechenland: nebst Darstellung und Erklärung vieler neuentdecken Denkmäler griechischen Styls, und einer kritischen Übersicht aller Unternehmungen dieser Art von Pausanias bis auf unsere Zeiten. Paris: Cotta; 1830.
5. Brøndsted PO. (in French) Travels in Greece accompanied by archaeological research, and followed by an overview of all the scientific enterprises that have taken place in Greece from Pausania's to the present day. Voyages dans la Grece accompagnes de recherches archeologuiques, et suivis d'un apercu sur toutes les entreprises scientifiques qui ont eu lieu en Grece depuis Pausanias jusqu'a nos jours: Paris: Didot; 1830.
6. Bobé L. (in Danish) Moritz Hartmann MDCLVI-MDCXCV: Danish and Venetian war captain, knight of San Marco and governor in Trankebar: Denmark's relations with the Republic of Venice. Moritz Hartmann MDCLVI-MDCXCV: dansk og venetiansk orlogskaptajn, ridder af San Marco og gouverneur i Trankebar: Danmarks forbindelser med Republiken Venedig. Copenhagen: Levin og Munksgaards Forlag; 1933.
7. Gjörwell CG. (in Swedish) Anna Åkerström. Det Svenska Biblioteket, Tredje Delen, Printed by Carl Gottlieb Ulf. Stockholm 1759.
8. Pensabene P, Gasparini E, editors. Interdisciplinary Studies on Ancient Stone. Proceedings of the X International Conference of ASMOSIA; 2014.
9. Jenkins ID, Middleton AP. Paint on the parthenon sculptures: part two—scientific aspects. BSA. 1988;83:183–207.
10. Penrose FC. An investigation of the Principles of Athenian Architecture. London1851.
11. Leibig JV. über den Thierschit. Justus Liebigs Ann Chem. 1853;86(1):113–5.
12. Pinna D, Galeotti M, Rizzo A. Brownish alterations on the marble statues in the church of Orsanmichele in Florence: what is their origin? Herit Sci. 2015;3:1–13.
13. Mas M, Jorge A, Gavilán B, Solís M, Parra E, Pérez P-P. Minateda rock shelters (Albacete) and post-palaeolithic art of the Mediterranean Basin in Spain: pigments, surfaces and patinas. J Archaeol Sci. 2013;40(12):4635–47.
14. Arrizabalaga I, Gómez-Laserna O, Aramendia J, Arana G, Madariaga JM. Applicability of a diffuse reflectance infrared Fourier transform handheld spectrometer to perform in situ analyses on cultural heritage materials. Spectrochim Acta Part A Mol Biomol Spectrosc. 2014;129:259–67.
15. Monico L, Rosi F, Miliani C, Daveri A, Brunetti BG. Non-invasive identification of metal-oxalate complexes on polychrome artwork surfaces by reflection mid-infrared spectroscopy. Spectrochim Acta Part A Mol Biomol Spectrosc. 2013;116:270–80.
16. Rosado T, Gil M, Mirão J, Candeias A, Caldeira AT. Oxalate biofilm formation in mural paintings due to microorganisms–a comprehensive study. Int Biodeterior Biodegrad. 2013;85:1–7.
17. Holclajtner-Antunović I, Stojanović-Marić M, Bajuk-Bogdanović D, Žikić R, Uskoković-Marković S. Multi-analytical study of techniques and palettes of wall paintings of the monastery of Žiča, Serbia. Spectrochim Acta Part A Mol Biomol Spectrosc. 2016;156:78–88.
18. González-Gómez W, Quintana P, Gómez-Cornelio S, García-Solis C, Sierra-Fernandez A, Ortega-Morales O, et al. Calcium oxalates in biofilms on limestone walls of Maya buildings in Chichén Itzá, Mexico. Environ Earth Sci. 2018;77:1–12.
19. Del Monte M, Sabbioni C, Zappia G. The origin of calcium oxalates on historical buildings, monuments and natural outcrops. Sci Total Environ. 1987;67(1):17–39.
20. Di Bonaventura MP, Del Gallo M, Cacchio P, Ercole C, Lepidi A. Microbial formation of oxalate films on monument surfaces: bioprotection or biodeterioration? Geomicrobiol J. 1999;16(1):55–64.
21. Gadd GM, Bahri-Esfahani J, Li Q, Rhee YJ, Wei Z, Fomina M, et al. Oxalate production by fungi: significance in geomycology, biodeterioration and bioremediation. Fungal Biol Rev. 2014;28(2–3):36–55.
22. Gadd GM. Fungal biomineralization. Curr Biol. 2021;31(24):R1557–63.
23. Polikreti K, Maniatis Y. Micromorphology, composition and origin of the orange patina on the marble surfaces of Propylaea (Acropolis, Athens). Sci Total Environ. 2003;308(1–3):111–9.
24. Maravelaki-Kalaitzaki P. Black crusts and patinas on Pentelic marble from the Parthenon and Erechtheum (Acropolis, Athens): characterization and origin. Anal Chim Acta. 2005;532(2):187–98.
25. Burgos-Cara A, Ruiz-Agudo E, Rodriguez-Navarro C. Effectiveness of oxalic acid treatments for the protection of marble surfaces. Mater Des. 2017;115:82–92.
26. King HE, Mattner DC, Plümper O, Geisler T, Putnis A. Forming cohesive calcium oxalate layers on marble surfaces for stone conservation. Cryst Growth Des. 2014;14(8):3910–7.
27. Meloni P, Manca F, Carcangiu G. Marble protection: an inorganic electrokinetic approach. Appl Surf Sci. 2013;273:377–85.
28. He L, Jiang Y, Ma W, Liu Y, Yang F, Lu R, et al. A new method to prepare calcium oxalate films for marble protection. Sci China Technol Sci. 2023;66(8):2237–45.
29. Rampazzi L. Calcium oxalate films on works of art: a review. J Cult Herit. 2019;40:195–214.
30. Hedegaard SB, Delbey T, Brøns C, Rasmussen KL. Painting the Palace of Apries II: ancient pigments of the reliefs from the Palace of Apries, Lower Egypt. Herit Sci. 2019;7(1):1–32.
31. Rasmussen KL, van der Plicht J, La Nasa J, Ribechini E, Colombini MP, Delbey T, et al. Investigations of the relics and altar materials relating to the apostles St James and St Philip at the Basilica dei Santi XII Apostoli in Rome. Herit Sci. 2021;9:1–30.
32. Boesenberg U, Henriksen C, Rasmussen KL, Chiang Y-M, Garrevoet J, Ravnsbæk DB. State of LiFePO4 Li-ion battery electrodes after 6533 deep-discharge cycles characterized by combined micro-XRF and micro-XRD. ACS Appl Energy Mater. 2022;5(4):4358–68.
33. Magrini D, Cantisani E, Vettori S, Rasmussen KL. Insights into Della Robbia's terracotta monument to cardinal federighi: raw materials and technologies. Appl Sci. 2022;12(9):4304.
34. Xiao J, Song Y, Li Y. Comparison of quantitative X-ray diffraction mineral analysis methods. Minerals. 2023;13(4):566.
35. Lluveras-Tenorio A, Andreotti A, Talarico F, Legnaioli S, Olivieri LM, Colombini MP, et al. An insight into gandharan art: materials and techniques of polychrome decoration. Heritage. 2022;5(1):488–508.
36. Orsini S, Parlanti F, Bonaduce I. Analytical pyrolysis of proteins in samples from artistic and archaeological objects. J Anal Appl Pyrolysis. 2017;124:643–57.

37. Orsini S, Yadav A, Dilillo M, McDonnell LA, Bonaduce I. Characterization of degraded proteins in paintings using bottom-up proteomic approaches: new strategies for protein digestion and analysis of data. Anal Chem. 2018;90(11):6403–8.

38. Lluveras-Tenorio A, Orsini S, Pizzimenti S, Del Seppia S, Colombini MP, Duce C, et al. Development of a GC–MS strategy for the determination of cross-linked proteins in 20th century paint tubes. Microchem J. 2021;170:106633.

39. Vinciguerra R, Galano E, Vallone F, Greco G, Vergara A, Bonaduce I, et al. Deglycosylation step to improve the identification of egg proteins in art samples. Anal Chem. 2015;87(20):10178–82.

40. Orsburn BC. Evaluation of the sensitivity of proteomics methods using the absolute copy number of proteins in a single cell as a metric. Proteomes. 2021;9(3):34.

41. Frankenfield AM, Ni J, Ahmed M, Hao L. Protein contaminants matter: building universal protein contaminant libraries for DDA and DIA proteomics. J Proteome Res. 2022;21(9):2104–13.

42. Zaru R, Orchard S, Consortium U. UniProt tools: BLAST, align, peptide search, and id mapping. Curr Protoc. 2023;3(3):e697.

43. Declercq A, Bouwmeester R, Chiva C, Sabidó E, Hirschler A, Carapito C, et al. Updated MS^{2}PIP web server supports cutting-edge proteomics applications. Nucleic Acids Res. 2023. https://doi.org/10.1093/nar/gkad335.

44. Sassoni E, Graziani G, Franzoni E, Scherer GW. Conversion of calcium sulfate dihydrate into calcium phosphates as a route for conservation of gypsum stuccoes and sulfated marble. Constr Build Mater. 2018;170:290–301.

45. Sassoni E. Hydroxyapatite and other calcium phosphates for the conservation of cultural heritage: a review. Materials. 2018;11(4):557.

46. Fassina V. New findings on past treatments carried out on stone and marble monuments' surfaces. Sci Total Environ. 1995;167(1–3):185–203.

47. Ransome F. Stone artificial, stone colouring, stone preserving. British patent. 1856;2267.

48. Monaco D, Saggioro F, Marrocchino E, Vaccaro C, Marchesini M. Archaeometric analysis of encrustations adhering to pietra ollare fragments from the medieval village of nogara. Heritage. 2023;6(4):3365–84.

49. Norton R, Roberts J, Huebert B. Tropospheric oxalate. Geophys Res Lett. 1983;10(7):517–20.

50. Martinelango PK, Dasgupta PK, Al-Horr RS. Atmospheric production of oxalic acid/oxalate and nitric acid/nitrate in the Tampa Bay airshed: parallel pathways. Atmos Environ. 2007;41(20):4258–69.

51. Corvo F, Reyes J, Valdes C, Villaseñor F, Cuesta O, Aguilar D, et al. Influence of air pollution and humidity on limestone materials degradation in historical buildings located in cities under tropical coastal climates. Water Air Soil Pollut. 2010;205:359–75.

52. Manninen S. Deriving nitrogen critical levels and loads based on the responses of acidophytic lichen communities on boreal urban Pinus sylvestris trunks. Sci Total Environ. 2018;613:751–62.

53. Brøns C, Rasmussen KL, Di Crescenzo MM, Stacey R, Lluveras-Tenorio A. Painting the Palace of Apries I: ancient binding media and coatings of the reliefs from the Palace of Apries, Lower Egypt. Herit Sci. 2018;6(1):1–20.

54. Brecoulaki H, Zaitoun C, Stocker SR, Davis JL, Karydas AG, Colombini MP, et al. An archer from the palace of Nestor: a new wall-painting fragment in the Chora Museum. Hesperia. 2008;77(3):363–97.

55. Brecoulaki H, Andreotti A, Bonaduce I, Colombini MP, Lluveras A. Characterization of organic media in the wall-paintings of the "Palace of Nestor" at Pylos, Greece: evidence for a secco painting techniques in the Bronze Age. J Archaeol Sci. 2012;39(9):2866–76.

56. Brecoulaki HS, Perdikatsis SV, Lluveras-Tenorio A, Bonaduce I, Colombini M. A technological investigation of the painting materials. In: Tournavitou I, editor. The Wall Paintings of the West House at Mycenae. Greece: INSTAP Academic Press (Institute for Aegean Prehistory); 2017.

57. Linn R, Bonaduce I, Ntasi G, Birolo L, Yasur-Landau A, Cline EH, et al. Evolved gas analysis-mass spectrometry to identify the earliest organic binder in aegean style wall paintings. Angew Chem. 2018;130(40):13441–4.

58. Kakoulli I. Late Classical and Hellenistic painting techniques and materials: a review of the technical literature. Stud Conserv. 2002;47(sup1):56–67.

59. Hu W, Zhang H, Zhang B. Identification of organic binders in ancient Chinese paintings by immunological techniques. Microsc Microanal. 2015;21(5):1278–87.

60. Liu L, Shen W, Zhang B, Ma Q. Microchemical study of pigments and binders in polychrome relics from Maiji Mountain Grottoes in Northwestern China. Microsc Microanal. 2016;22(4):845–56.

61. Ge R, Yang L, Shen M, Sun W. Investigating the composition and application of an ancient multipurpose material discovered on the Qin Terracotta Army statues. Archaeometry. 2022;64(2):422–37.

62. Ma Z, Yan J, Zhao X, Wang L, Yang L. Multi-analytical study of the suspected binding medium residues of wall paintings excavated in Tang tomb, China. J Cult Herit. 2017;24:171–4.

63. Bonaduce I, Blaensdorf C, Dietemann P, Colombini MP. The binding media of the polychromy of Qin Shihuang's Terracotta Army. J Cult Herit. 2008;9(1):103–8.

64. Lluveras-Tenorio A, Vinciguerra R, Galano E, Blaensdorf C, Emmerling E, Perla Colombini M, et al. GC/MS and proteomics to unravel the painting history of the lost Giant Buddhas of Bāmiyān (Afghanistan). PLoS ONE. 2017;12(4):e0172990.

65. Kouzeli K, Lazari C, Economopoulos A, Pavelis C, editors. Phosphatic patinas on Greek monuments (Acropolis of Athens and other ancient and Byzantine monuments): general discussion and further documentation on the presence of oxalates. International symposium (II): the oxalate films in the conservation of works of art, Milan, March 25–27, 1996 Proceedings; 1996.

66. Ariño X, Saiz-Jimenez C. Colonization and deterioration processes in Roman mortars by cyanobacteria, algae and lichens. Aerobiologia. 1996;12:9–18.

67. Garcia-Valles M, Urzì C, De Leo F, Salamone P, Vendrell-Saz M. Biological weathering and mineral deposits of the Belevi marble quarry (Ephesus, Turkey). Int Biodeterior Biodegr. 2000;46(3):221–7.

68. De La Rosa JPM, Warke PA, Smith BJ. Lichen-induced biomodification of calcareous surfaces: bioprotection versus biodeterioration. Prog Phys Geogr. 2013;37(3):325–51.

69. Edwards H, Russell N, Seaward M. Calcium oxalate in lichen biodeterioration studied using FT-Raman spectroscopy. Spectrochim Acta Part A Mol Biomol Spectrosc. 1997;53(1):99–105.

70. Edwards H, Farwell D, Seaward M, Giacobini C. Preliminary Raman microscopic analyses of a lichen encrustation involved in the biodeterioration of Renaissance frescoes in central Italy. Int Biodeterior. 1991;27(1):1–9.

Publisher's Note